

The British University in Egypt

BUE Scholar

Nanotechnology Research Centre

Research Centres

Summer 9-25-2023

iCVD Polymer Thin Film Bio-Interface-Performance for Fibroblasts, Cancer-Cells, and Viruses Connected to Their Functional Groups and In Silico Studies

Torge Hartig

Chair for Multicomponent Materials Department of Materials Science Kiel University 24143 Kiel, Germany,
toha@tf.uni-kiel.de

Asmaa T. Mohamed

Nanotechnology Research Centre (NTRC) The British University in Egypt (BUE),
asmaa.mohamed@bue.edu.eg

Nasra F. Abdel Fattah


Virology and Immunology Unit Cancer Biology Department National Cancer Institute Cairo University,
nasra_fathy87@yahoo.com

Aydin Gülses

Department of Oral and Maxillofacial Surgery Campus Kiel University Hospital of Schleswig-Holstein
24105 Kiel, Germany, Aydin.Guelses@uksh.de

Follow this and additional works at: https://buescholar.bue.edu.eg/nanotech_research_centre

Tim Tjardts

 *Chair for Multicomponent Materials Department of Materials Science Kiel University 24143 Kiel, Germany,*
tt@tf.uni-kiel.de

Recommended Citation

Hartig, Torge; Mohamed, Asmaa T.; Abdel Fattah, Nasra F.; Gülses, Aydin; Tjardts, Tim; Kangah, Esther Afiba; Gabriel Chan, Kwing Pak; Salih Veziroglu, Salih; Acil, Yahya; Aktas, Oral Cenk; Jörg Wiltfang, Jörg; Loutfy, Samah A.; Strunskus, Thomas; Faupel, Franz; Amin, Amal; and Schröder, Stefan, "iCVD Polymer Thin Film Bio-Interface-Performance for Fibroblasts, Cancer-Cells, and Viruses Connected to Their Functional Groups and In Silico Studies" (2023). *Nanotechnology Research Centre*. 68.
https://buescholar.bue.edu.eg/nanotech_research_centre/68

This Article is brought to you for free and open access by the Research Centres at BUE Scholar. It has been accepted for inclusion in Nanotechnology Research Centre by an authorized administrator of BUE Scholar. For more information, please contact bue.scholar@gmail.com.

Authors

Torge Hartig, Asmaa T. Mohamed, Nasra F. Abdel Fattah, Aydin Gülses, Tim Tjardts, Esther Afiba Kangah, Kwing Pak Gabriel Chan, Salih Salih Veziroglu, Yahya Acil, Oral Cenk Aktas, Jörg Jörg Wiltfang, Samah A. Loutfy, Thomas Strunskus, Franz Faupel, Amal Amin, and Stefan Schröder

iCVD Polymer Thin Film Bio-Interface-Performance for Fibroblasts, Cancer-Cells, and Viruses Connected to Their Functional Groups and In Silico Studies

Torge Hartig, Asmaa T. Mohamed, Nasra F. Abdel Fattah, Aydin Gülses, Tim Tjardts, Esther Afiba Kangah, Kwing Pak Gabriel Chan, Salih Veziroglu, Yahya Acil, Oral Cenk Aktas, Jörg Wiltfang, Samah A Loutfy, Thomas Strunskus, Franz Faupel, Amal Amin, and Stefan Schröder*

Thin polymer coatings are used to improve the interface between biological species and functional materials. Their interaction is significantly influenced by the functional groups and roughness of the polymer film and prediction of the interaction is thus of great interest. However, for conventional polymer films, this cannot be examined independently because of the interplay of defects, residual solvent molecules, roughness, and functional groups. Solvent-free polymer films prepared by initiated chemical vapor deposition (iCVD) exhibit conformal, defect-free characteristics and enable precise tailoring of the functional groups. This facilitates to isolate the contribution of functional groups on the bio-interface performance. Consequently, in silico studies can enable a prediction of ligand interaction in anti-viral activity for SARS-CoV-2 based on defined polymer and key protein structures. Furthermore, the cell viability of human fibroblasts can be traced back to the functional groups of the repeating units. For human liver cancer cell culture, it turns out that more sophisticated models are needed. The insilico-iCVD approach can enable precise tailoring of complex polymer films optimized for the respective interfaces. In addition, this first big scan of the bio-interface performance of iCVD films enables a solid starting point in areas like anticancer, antiviral, and biocompatibility for future studies.

1. Introduction

Functional polymers are widely used in biomedical applications, which require precise material characteristics like roughness and surface functionality due to the complex nature of biological pathways, specific cells, viruses, and other biological species. Functional polymers can be natural, synthetic, or blends to combine the merits of both worlds.^[1] In the form of thin films, they enable unique properties in industry and especially in the biomedical fields such as in drug delivery,^[2–4] dye and heavy metal ion removal,^[5,6] tissue engineering,^[7,8] biosensors^[9,10] and many more. To precisely tailor such polymer thin films, especially vapor phase deposition techniques are attractive as they present the most controlled growth in polymerization while being solvent-free.^[11] Compared to other vapor phase methods, initiated chemical vapor deposition (iCVD) represents

T. Hartig, T. Tjardts, K. P. G. Chan, S. Veziroglu, O. C. Aktas, T. Strunskus, F. Faupel, S. Schröder
 Chair for Multicomponent Materials
 Department of Materials Science
 Kiel University
 24143 Kiel, Germany
 E-mail: ssch@tf.uni-kiel.de

A. T. Mohamed, S. A. Loutfy
 Nanotechnology Research Centre (NTRC)
 The British University in Egypt (BUE)
 El-Sherouk City, Cairo 11837, Egypt

N. F. A. Fattah, S. A. Loutfy
 Virology and Immunology Unit
 Cancer Biology Department
 National Cancer Institute
 Cairo University
 Fom El-Khalig, Cairo 11796, Egypt

A. Gülses, E. A. Kangah, Y. Acil, J. Wiltfang
 Department of Oral and Maxillofacial Surgery
 Campus Kiel
 University Hospital of Schleswig-Holstein
 24105 Kiel, Germany

The ORCID identification number(s) for the author(s) of this article can be found under <https://doi.org/10.1002/admi.202300587>

© 2023 The Authors. Advanced Materials Interfaces published by Wiley-VCH GmbH. This is an open access article under the terms of the Creative Commons Attribution License, which permits use, distribution and reproduction in any medium, provided the original work is properly cited.

DOI: 10.1002/admi.202300587

the perfect technique to precisely tailor nanoscale homopolymer as well as copolymer surface coatings,^[12–14] which meet the high requirements for biomedical environments and which can furthermore be upscaled to large industrial process lines.^[15–18] This is possible because the (co-)monomer vapor flows can be adjusted precisely, leading to tailored polymer compositions, while the resulting thin films exhibit pin-hole-free and highly conformal properties on the nanometer scale.^[19,20] The well-understood gas phase kinetics enable advanced ways to produce highly specific nanometer thin coatings like, e.g., gradient structures.^[21,22] Only limited by the vacuum vapor phase behavior, the biocompatible polymers used in iCVD can be combined on demand and range from organosilicons^[23,24] over hydrogels^[25,26] to carbohydrates.^[27] In iCVD especially hydrogels have successfully been used in bio-interface applications like advanced cell culture platforms,^[28] for bone tissue engineering,^[29] or as antifouling coatings.^[30]

Nevertheless, studies of the bio-interface behavior of iCVD thin films are usually collaborations between the bio-/medical fields and chemical engineering fields and especially new monomer installation can require a long time and effort, making the choice of suitable monomers difficult. Thus, it is of great interest to perform a preliminary screening of biocompatible iCVD polymers to see which ones are suitable for specific applications and to see if the bio-interface performance can be predicted. It is also of high interest to see if an exploratory tool like an *in silico* study^[31] can be used to choose from the growing palette of possible iCVD polymers^[32–34] beforehand. For this purpose, three different biological applications for the polymer thin films were considered in this study. For anticancer cell culture tests and antiviral ligand interaction including SARS-CoV-2, the interface performance was simulated *in silico*. Furthermore, human fibroblasts were used for biocompatibility tests where the results were discussed regarding the different functional groups of the polymers.

Synthetic polymers can be bioactive in all three named applications depending on the macromolecular structure as well as the repeating units.^[35] Biocompatible synthetic polymers commonly include polar groups in their repeating units leading to good wetting behavior, while amines can strongly enhance cell-polymer interactions.^[36] Antiviral polymers can have various mechanisms of action in blocking certain steps of the viral replication cycle while not affecting the function of the host cell. The most material-dependent approach is the use of an antiviral agent to bind viruses.^[37] Synthetic polymers are highly interesting for this approach as their tunability in structure and functional groups can be optimized for interaction with a virus.^[38] Repeating units with an amine functionality are popular in designing antiviral

synthetic polymers.^[39] Furthermore, polymers, like polyphenols, can be applied in anticancer applications via different pathway inhibitions.^[40]

Regarding the three named applications this study investigates well-known biocompatible iCVD monomers with different functional groups, namely HEMA (2-hydroxyethyl methacrylate),^[29] DMAEMA (2-(dimethylamino)ethyl methacrylate),^[30] EGDMA (ethylene glycol dimethacrylate)^[41] and V3D3 (1,3,5-trivinyl-1,3,5-trimethylcyclo-trisiloxane).^[42,43] They were combined in every possible way, always in 1/3 hydrogel 2/3 crosslinker combinations to be comparable, as well as homopolymers of the crosslinkers.

The resulting polymer thin films were precisely analyzed and examined in the abovementioned three different biological environments as displayed in **Figure 1**.

2. Results and Discussion

2.1. Characterization of Polymer Materials

The deposited polymer thin films were analyzed by Fourier-transform infrared (FTIR) spectroscopy, X-ray photoelectron spectroscopy (XPS), atomic force microscopy (AFM), water contact angle (WCA) measurements, variable angle spectroscopic ellipsometry (VASE) and profilometry. The FTIR spectra of the polymer thin films are shown in **Figure 2a**. The absence of bands above 3000 cm⁻¹ indicates a successful polymerization during the iCVD process.^[44] The strong characteristic carbonyl peak \approx 1700 cm⁻¹ was observed in all polymers including EGDMA. Other characteristic peaks were observed at 1250 cm⁻¹ for the Si- and at 1000 cm⁻¹ for the Si—O—Si bond for V3D3 containing polymers. The hydroxyl groups of the HEMA-containing copolymers were identified between 3150 cm⁻¹ and 3600 cm⁻¹. The ternary characteristic nitrogen group of the DMAEMA monomer was not clearly identified in FTIR because of the low film thickness (below 300 nm), high cross-linking, and weak IR interaction of this group.^[44] While FTIR is traditionally used to determine copolymer ratios in iCVD polymers^[29] a surface-sensitive chemical analysis with XPS is more relevant for this study, as surface interactions are examined. Via XPS the characteristic nitrogen was identified to be present at the surface as shown in **Figure 2b**.

XPS measurements were performed to confirm the chemical surface composition of the deposited polymer films. The high-resolution peaks used for the determination of the copolymer structures can be found in Supporting Information S1. For the p(DMAEMA-co-EGDMA) thin film, the atomic percentages for N, O, and C were 3.06%, 29.68%, and 67.26%, respectively which were referred to 69% EGDMA and 31% DMAEMA in the copolymer by calculation with respect to the monomer structures. For p(DMAEMA-co-V3D3), the atomic percentages for Si, N, O, and C were 14.09%, 2.20%, 28.42%, and C 55.29%, respectively referring to 68% of V3D3 and 32% DMAEMA. For p(HEMA-co-V3D3) the atomic percentage for C=O was 3.21% with Si—O at 18.13%. This leads to a percentage of 65% V3D3 and 35% HEMA. The O 1s subpeak was used to determine Si—O content.^[45] For p(HEMA-co-EGDMA) the determination of the comonomer percentage is not as trivial as for the aforementioned polymers. Here the same functional groups are present in both comonomers. Both have carbonyl groups and hydroxyl groups. The percentages

S. Veziroglu, O. C. Aktas, T. Strunskus, F. Faupel, S. Schröder
Kiel Nano
Surface and Interface Science KiNSIS
Kiel University
24118 Kiel, Germany
A. Amin
Polymers and Pigments Department
Chemical Industries Research Institute
National Research Centre
Giza 12622, Egypt

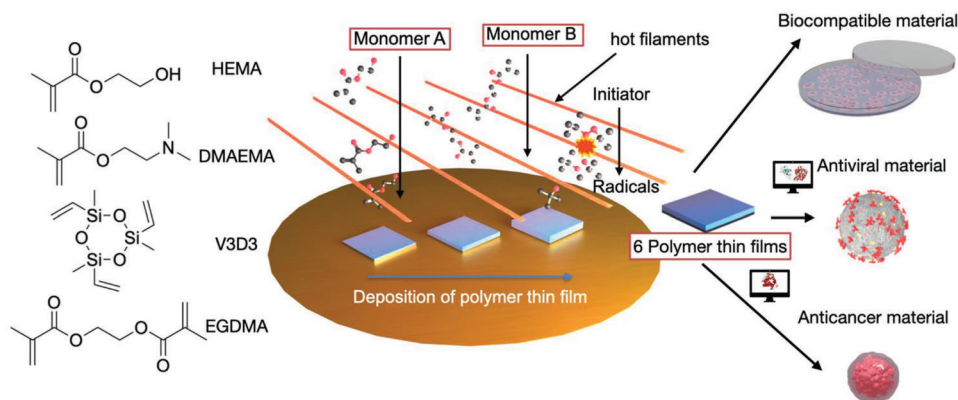


Figure 1. The structural formulas on the left show the different monomers used in this study. The process of iCVD is used to deposit six different polymer thin films based on the different (co-)monomers. The resistively heated filaments decompose the initiator, in this case TBPO (*tert-butyl-peroxide*), into free radicals. Monomer molecules adsorb on the cooled sample stage and the free radicals initiate a free radical polymerization at the substrate stage. By combining the different (co-)monomers in iCVD different (co-)polymers with different functional groups are deposited as conformal thin films. These films were finally analyzed regarding their bio-interface behavior. The biocompatibility was tested by different cell viability tests. The antiviral behavior including *in silico* computational docking score analysis regarding the SARS-CoV2 spike protein and ACE-2 (angiotensin-converting enzyme 2) enzyme, representing a binding site at the cell membrane for the virus, was tested. Furthermore, the anticancer behavior was tested including docking score analysis with the apoptotic pathway regulator BCL2 (b-cell lymphoma 2).

of these functional groups in the polymer can only be determined by deconvolution of the shoulder peak, which cannot be done with satisfying precision. Due to the precision in copolymer percentages for the other copolymers, this copolymer is treated with a 33%+–10% HEMA to 67%+–10% EGDMA content inside this study.

The water contact angles were determined for the polymer thin films on silicon wafers as indicated in Figure 2c and supplementary information S2 in order to find a possible relation between wetting and the bio-interface performance. The copolymer thin films had lower contact angles as expected compared to the homopolymers, as HEMA and DMAEMA are more hydrophilic compared to V3D3 and EGDMA. For p(DMAEMA-co-V3D3), the wetting showed no significant difference with respect to the homopolymer of pV3D3. The relatively high water contact angles with respect to other hydrogel copolymers result from the high cross-linking of 2/3.

Since the roughness has a significant influence on the bio-interface performance it is investigated via AFM. For all samples, AFM measurements confirmed a smooth surface of a maximum 2.17 nm root mean square roughness (RMS) as seen in Figure 2d. Interestingly for p(DMAEMA-co-V3D3), a pattern on the very low nanoscale was observed, showing regularity in larger scans as seen in the Supporting Information S2. This cannot be compared to any other work done on this copolymer as to our knowledge it is deposited for the first time within this study. The more hydrophobic V3D3 comonomer could potentially dominate the wetting behavior in this copolymer fitting the AFM and XPS measurements to the measured WCAs. Generally, V3D3-containing polymer thin films show a surface pattern in the high nanometer range in the *x*, *y*-direction, while this is not observed in EGDMA-containing polymer films. The height of the topography is not noticeably different in any of the examined thin films. The material analysis via AFM, FTIR, XPS, and WCA measurements shows that the iCVD films have minimal roughness and present a perfect basis for analyzing the impact of functional groups on the

bio-interface behavior excluding the influence of different morphologies.

2.2. Biological Studies

2.2.1. *In Silico* Study For Anticancer and Antiviral Interactions

Regarding the biological characterization, the molecular docking was calculated for the polymer thin films of pV3D3, p(DMAEMA-co-V3D3), p(HEMA-co-V3D3), pEGDMA, p(DMAEMA-co-EGDMA), and p(HEMA-co-EGDMA) for SARS-COV2 spike protein, human ACE2 protein, and Bcl2 protein. Molecular docking calculations showed a favorable interaction of ligands against ACE2 protein (PDB ID: 1R42), SARS-COV2 Spike protein (PDB ID: 6vw1), and Bcl2 protein (PDB:2W3L) for all produced polymer films. These results are presented in Table 1. P(DMAEMA-co-EGDMA) turned out to be the best-performing copolymer thin film. The respective results are shown in Figure 3 and Table 2. The other models are provided in the Supporting Information S4.

Figure 3a shows the docking score experiments with the SARS-CoV2 spike protein, while Figure 3b,c shows the docking score experiments with Angiotensin-converting enzyme 2 and B-cell lymphoma 2, respectively. The docking experiments were performed using the H-dock web server tool. The results have 2 different values, where the docking energy score is based on the Fast Fourier Transform (FFT) global docking scoring function (HDOCK lite) developed by the same developer. The docking energy score based on HDOCK ranked the best 10 models and docking poses between ligand and protein receptors and the best (lowest energy) mode. Therefore, the results were ranked and compared with Remdesivir as the standard drug. The root-mean-square deviation (RMSD) obtains the distance per angstrom between input ligands in the grid dimensions. The docking scores were ranked based on the standard docking score of “Remdesivir”.

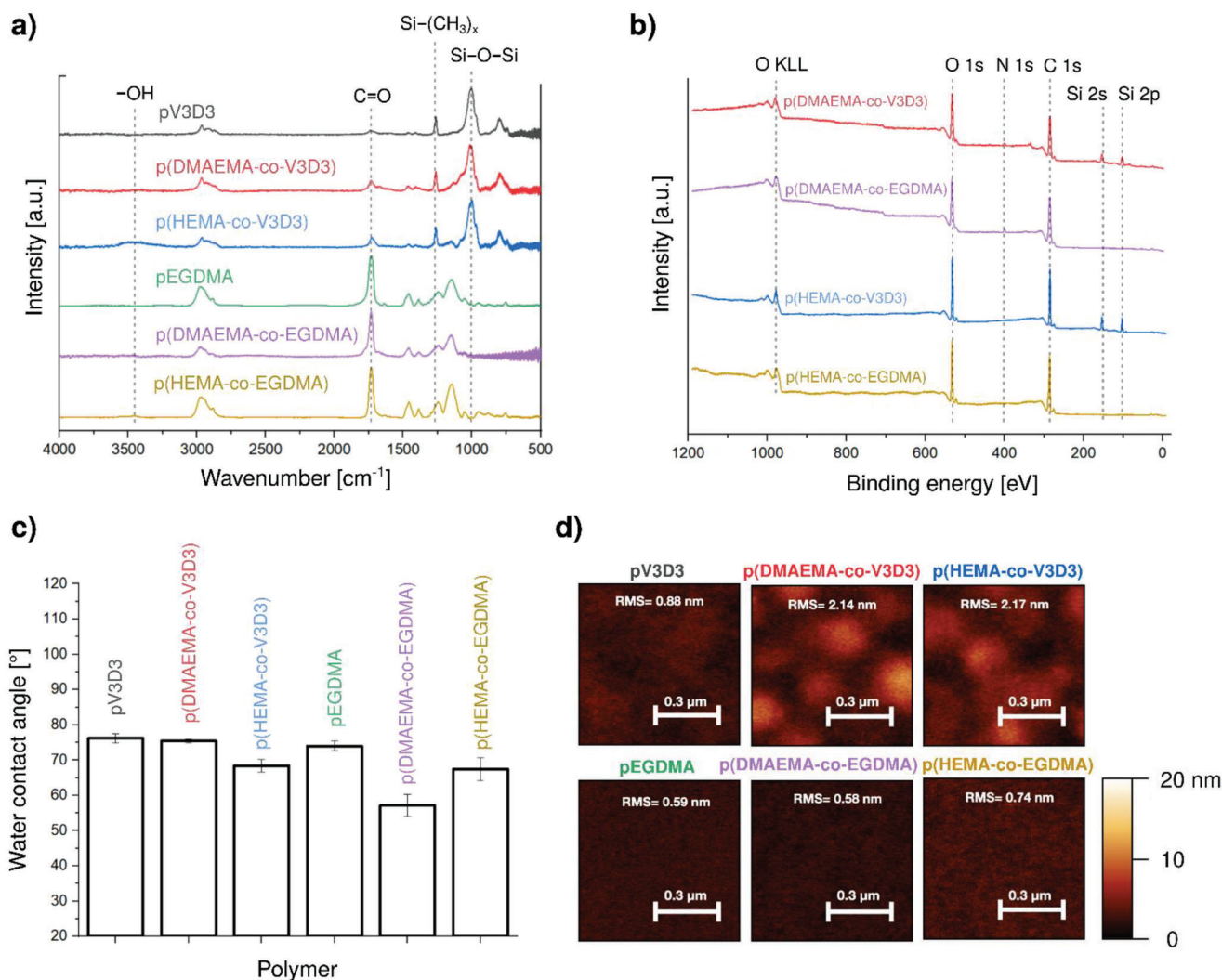


Figure 2. a) FTIR and b) XPS spectra of the polymers using V3D3 comonomer and EGDMA comonomer. C1s, N1s, and Si2p high-resolution peaks from XPS are provided in the supporting information S1. c) Water contact angles of the different polymer thin films and d) AFM measurements of the thin film surfaces including their root mean square roughness.

The *in silico* method was used as an exploratory tool to see if the performance of iCVD thin films in a complex bio-environment can be predetermined. Based on the modeled functional group's ligand interaction with key proteins of biological processes the method was successful in predetermining the most

successful antiviral thin film against SARS-CoV-2, p(DMAEMA-co-EGDMA), where the testing method relied on the ligand-protein interaction. For the even more complex example of the anticancer tests in cell culture the *in silico* results were no help to predetermine the thin film's performance. This can be attributed

Table 1. Molecular docking for the tested materials against spike protein of SARS-CoV2, ACE2, and BCL2 target proteins.

Protein/ ligand	Remdesivir (control)	pV3D3	p(DMAEMA-co-V3D3)	p(HEMA-co-V3D3)	pEGDMA	p(DMAEMA-co-EGDMA)	p(HEMA-co-EGDMA)
Spike	Docking Score	-177.98	-85.22	-127.15	-118.41	-119.11	-152.70
	Ligand RMSDs (Å)	208.29	207.93	207.43	207.07	205.65	208.01
ACE2	Docking Score	-213.30	-91.08	-133.39	-135.83	-114.03	-175.68
	Ligand RMSDs (Å)	197.60	194.63	195.59	197.86	192.49	195.85
BCL2	Docking Score	-172.91	-74.86	-109.32	-106.48	-92.32	-138.78
	Ligand RMSDs (Å)	19.93	9.91	21.70	21.13	22.04	21.79

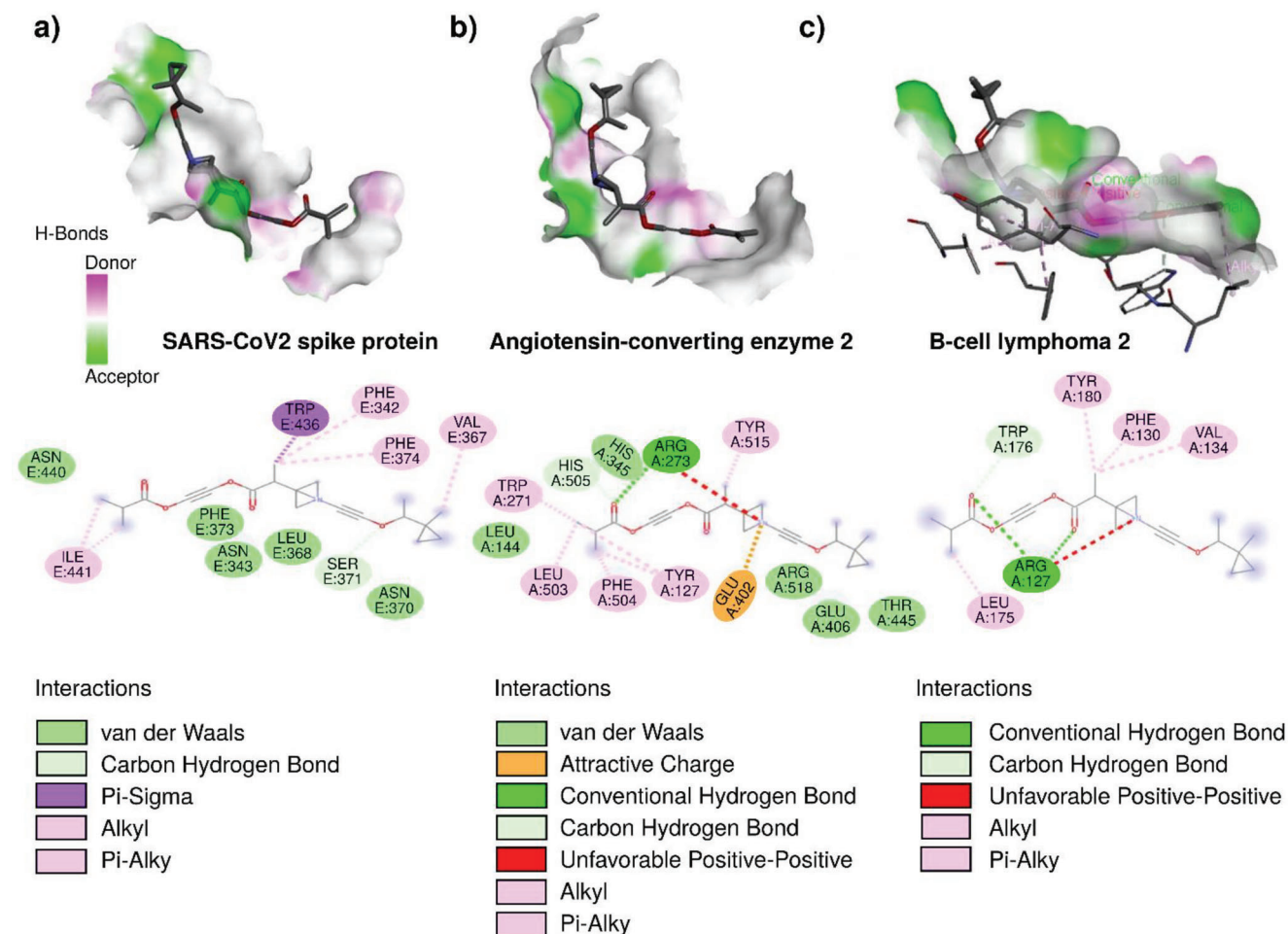


Figure 3. Example of modeled p(DMAEMA-co-EGDMA) docking score experiments with a) SARS-CoV2 spike protein, b) Angiotensin-converting enzyme 2, and c) B-cell lymphoma 2.

to the increased complexity of the experiments and many more possible pathways for cell death than the examined one.

2.2.2. Anti-Cancer Activity of Polymer Thin Films Against HepG2 and MCF-7

To test if the materials are applicable for biological applications in the respective anticancer and antiviral tests, MTT colorimetric as-

Table 2. Amino acids interactions and the bond types with p(DMAEMA-co-EGDMA) ligand.

Pocket amino acid	Interaction
Val 367	Conventional hydrogen bond as strong covalent bond associated between h bond donor and h bond acceptor
Phe 373 and Phe 374	Alkyl alkyl hydrophobic interaction and pi-sigma covalent bonding
TRP 436 and ILE 441	Alkyl bonding
ASN 343	Carbon hydrogen bonding

says with different application-specific cell lines were performed preliminary to check for the feasibility of the tested applications. The results can be seen in the Supporting Information S3. Since the tested materials showed more toxicity against the proliferation of HepG2 cells than MCF7 cells, cell migration assays and apoptotic gene expression involved in the mitochondria intrinsic apoptotic pathway were performed on the HepG2 cell line.

The results of cell migration experiments show that the investigated iCVD films are able to inhibit cell migration and proliferation after the second day of treatment. Further details are provided in the Supporting Information S5. Molecular investigations for the apoptotic effect induced by the tested materials on hepG2 using quantitative real-time polymerase chain reaction (PCR) showed that mRNA expressions of caspase 3 and Bax genes were downregulated after 24 h of cell exposure except for p(HEMA-co-EGDMA). In contrast, the effect of the investigated films on gene expression of BCL2 is upregulated in all tested materials except for p(HEMA-co-V3D3) and pEGDMA, where the BCL2 gene is downregulated as seen in Table 3.

The resulting data shows that the materials exerted their antiproliferative activity differently, depending on the respective functional groups of the polymer and their ability to interact with

Table 3. Quantitation of apoptotic gene expression after 24 h of cell exposure (Caspase, Bax, and anti-apoptotic BCL2) on a transcriptional level.

Treatment	Caspase 3 RQ 2- $\Delta\Delta CT$	BCL2 RQ 2- $\Delta\Delta CT$	Bax RQ 2- $\Delta\Delta CT$
Cell control	1	1	1
pV3D3	0.0011	3.16	0.48
p(DMAEMA-co-V3D3)	0.0004	3.07	0.18
p(HEMA-co-V3D3)	0.00029	0.35	0.033
pEGDMA	0.21	0.85	0.40
p(DMAEMA-co-EGDMA)	0.072	4.59	0.036
p(HEMA-co-EGDMA)	7.11	9.1	1.41
Positive control Paclitaxel (24 μ M)	0.04	34.77	0.21

apoptotic proteins, and shows that the mechanism of apoptosis is not via the mitochondria intrinsic apoptotic pathway. Therefore, further insight analysis to cover all apoptotic genes is needed to explore the exact mechanisms by which these materials exert their antitumor activity and determine effective target proteins used to control cancer disease.

2.2.3. Anti-Viral Activity of Polymer Thin Films Against Human Adenovirus-5 and SARS-CoV2

At first tests regarding antiviral activity of the materials against human adenovirus type 5 are performed on Vero cells. The results show that all tested materials inhibited the entry of the virus into the cells via results of the adsorption antiviral mechanism except p(DMAEMA-co-V3D3) which however shows antiviral activity in the virucidal antiviral mechanism as evidenced by an undetected level of viral copies using quantitative real-time PCR assay. In contrast, pEGDMA shows antiviral activity through the adsorption mechanism but not via the virucidal antiviral mechanism. This indicates the relevance of testing all possible antiviral mechanisms before proposing the general antiviral activity of any tested material. Further details are presented in the Supporting Information S6. In general, the antiviral activity can be explained in terms of the nature of the polymer structures and its high affinity to host receptors thus interrupting the binding of the virus to its receptor. This prevents viral entry and its pathogenic effect on cells. The charges of the tested compounds may bind to the viral DNA affecting its replication into cells exerting as shown in the virucidal mechanism. Moreover, the nature of polymer compounds can denature viral proteins or trap virions and prevent their availability inside cells and in turn their replication.^[31,46]

The polymer thin films are also tested against SARS-CoV2 using the CoviDrop SARS-CoV-2 Spike-ACE2 Binding Inhibitor Screening Assay. All materials show an inhibitory effect against the spike protein of SARS-CoV2 except p(HEMA-co-EGDMA) which shows no antiviral activity, which may need further investigations before excluding an antiviral activity against SARS-CoV2. The highest binding affinity was observed for p(DMAEMA-co-EGDMA). The results are shown in **Table 4**.

To summarize the antiviral testing all tested materials could inhibit the entry of adenovirus 5 into the cells which are used as a respiratory virus model. This was evidenced by results test-

ing the adsorption mechanism except p(DMAEMA-co-V3D3), which demonstrated neutralization to viral infectivity via virucidal mechanism as evidenced by undetectable viral copies from quantitative real-time PCR.

Regarding antiviral activities against the spike protein of SARS-CoV2, all tested materials show antiviral activities except p(HEMA-co-EGDMA) but further investigations are needed before excluding the antiviral activity of this material as this study only examines interaction with only spike protein not against other proteins in the whole virus.

2.2.4. Biocompatibility Tests for Human Fibroblast Cells

In the next step, the cell viability of the respective iCVD films is tested. The MTT assay as seen in **Figure 4a** shows that the cells cultured on the polymer thin films show superior cell viability compared to the control group, which approves the biocompatibility of all experimented materials. Despite nearly identical values, the highest cell metabolic activity was detected in pV3D3, followed by p(HEMA-co-EGDMA), pEGDMA, p(DMAEMA-co-V3D3), p(DMAEMA-co-V3D3) and p(DMAEMA-co-EGDMA), respectively.

Non-quantitative assessment via fluorescence images recorded at an examination period of 24 h indicates that fibroblasts cultured on all study samples tend to exhibit a higher

Table 4. Antiviral activity of polymer iCVD thin films against SARS-CoV2 via CoviDrop test.

Serial	Reads at 450 nm with an optional reference wavelength of 655 nm	Binding Inhibition%
Blank	0.024	–
BIC Strong	0.02	33.3
BIC Weak	0.018	0
Sample Wells Without Inhibitor	0.018	–
pV3D3	0.024	100
p(DMAEMA-co-V3D3)	0.02	33.3
p(HEMA-co-V3D3)	0.024	100
pEGDMA	0.025	116
p(DMAEMA-co-EGDMA)	0.028	166.6
p(HEMA-co-EGDMA)	0.018	0

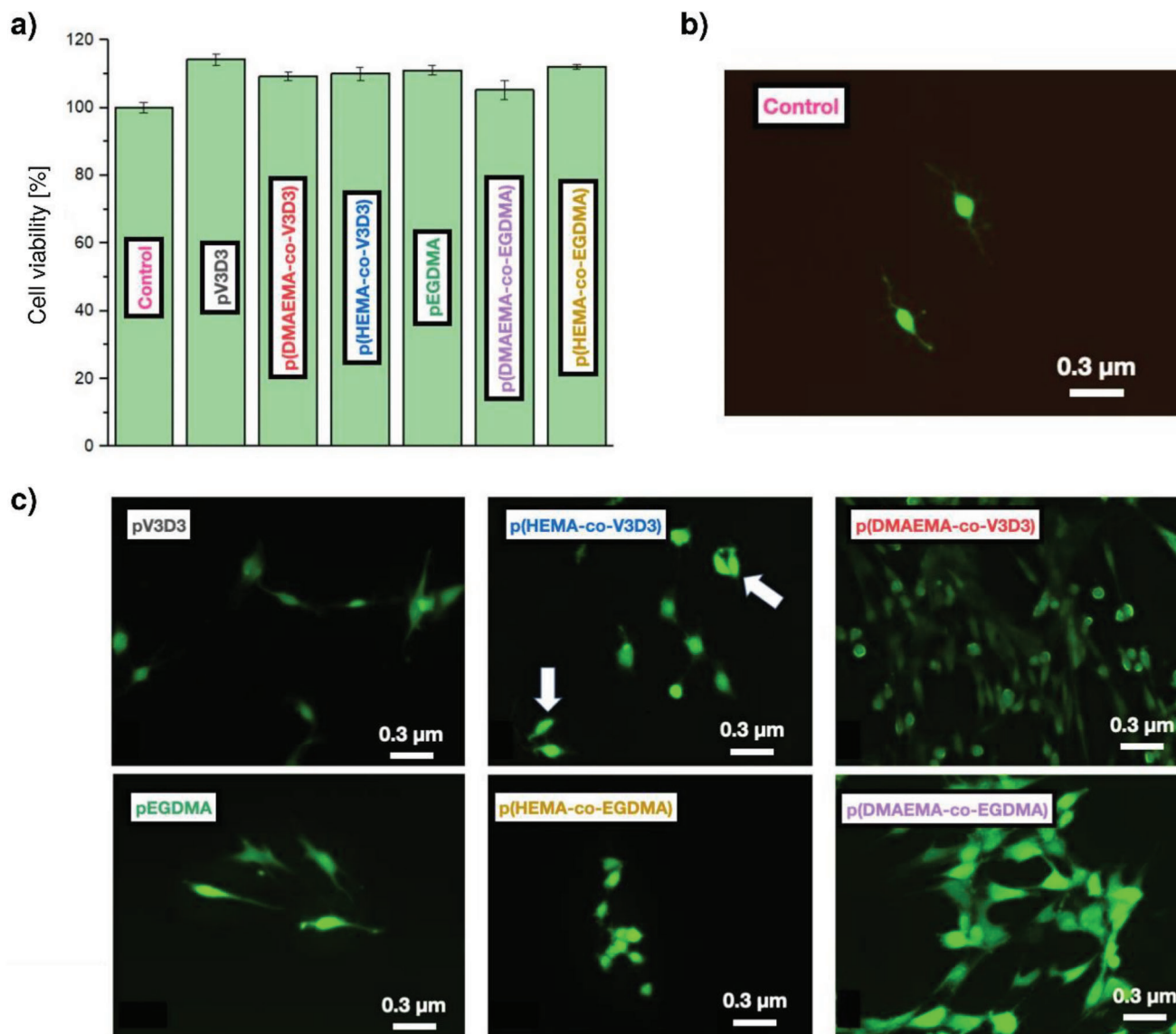


Figure 4. a) MTT assay of human fibroblasts on polymer thin film samples. b) Control fluorescence images and c) fluorescence images of immunostained fibroblasts for qualitative assessment of fibroblasts on the iCVD thin films. All tests were performed with bare glass as a control. Almost all cells present well-spread morphologies, whereas the white arrows show daughter cells on p(HEMA-co-V3D3) after mitosis. p(DMAEMA-co-EGDMA), p(DMAEMA-co-V3D3), and particularly p(HEMA-co-EGDMA) subgroups show an increased number of filopodia-like extensions and intercellular connections which also lead to cluster formation.

number of viable cells compared to those cultured on cells of the control group, shown in Figure 4b,c. Overall, non-vital cells could not be detected. Nearly all fibroblasts presented a well-spread morphology.

p(DMAEMA-co-EGDMA) and p(DMAEMA-co-V3D3) groups show superior cell viability via cell connections and colonization compared to the HEMA-based copolymers and PV3D3 and PEGDMA homopolymers considering the increased number of filopodia-like extensions and intercellular connections which also lead to cluster formations. Almost all cells present well-spread morphologies, whereas the white arrows highlight mitotic daughter cells on p(HEMA-co-V3D3) after cytokinesis. Despite appropriate viability and in-

tercellular connections among all study groups, p(DMAEMA-co-EGDMA) and p(HEMA-co-EGDMA) show significantly superior viability compared to pEGDMA. Similarly, p(DMAEMA-co-EGDMA) exhibits superior qualitative viability compared to p(HEMA-co-EGDMA) and pEGDMA. The labeling of the cells in HEMA-co-EGDMA, DMAEMA-co-EGDMA, DMAEMA-co-V3D3, and HEMA-co-V3D3 subgroups was in accordance with normal resting or actively growing cells that exist in a state known as interphase of the mitosis. Overall, V3D3- and EGDMA-based copolymers that contain DMAEMA result in an increased number of filopodia-like structures which approves a better cell communication. As HEMA and DMAEMA only differ in one functional group the difference

can clearly be attributed to the presence of the tertiary amino group of DMAEMA versus the hydroxyl group of HEMA.

3. Conclusion

Polymer thin film response in biological environments is of great interest for applications but is hard to predict due to the complex interaction pathways of biological species. Polymer films fabricated via iCVD were tested as a model system in this study to improve the understanding of the influence of different functional groups. In silico was successful in the exploratory prediction of the best-performing polymer thin film in p(DMAEMA-co-EGDMA) here shown for antiviral ligand interaction regarding SARS-CoV-2. Further insight investigations into cell culture are needed to verify the possible antiviral activity of the polymer thin films against SARS-CoV2.

Moreover, the polymer thin films were tested in anticancer behavior against human liver cancer cells. All polymer thin film compositions showed antiproliferative behavior. The results for the interaction of the polymers with BCL2 modeled in silico did not fit the experimental results, hinting at the cell culture being a too complex environment for such a simple simulation.

Further studies are required to explore the exact mechanisms of the complex antiproliferative activity of the materials against human liver cancer cells to determine the active target proteins that can be used to control such chronic disease and with that optimize the copolymer for the application. Future studies will analyze the cell cycle of the cancer cells, possible angiogenesis inhibition, DNA damage induction, telomerase activity, or epigenetic modifications before possible testing in vivo. Generally, the study has shown that wherever polymer ligand interaction or other complex requirements are of strong interest in silico could in the future be used to model a large amount of possible iCVD thin film compositions. This could be used to examine the most promising polymers, even considering, e.g., terpolymers from a larger number of monomers, with traditional iCVD research mainly working with one or two monomers. The polymer films tested in this study can open new pathways in applications against cancer proliferation to prevent metastasis, in antiviral applications^[47,48] like high maintenance surfaces,^[49] or for drug delivery.^[50,51] Furthermore, for human fibroblast cell viability, the trends could be traced back directly to the functional groups of the repeating units of the iCVD thin films, with DMAEMA copolymers performing the best, suggesting future use in accompanied applications.

4. Experimental Section

Polymer Thin Film Deposition Method: The used chemicals for the polymer thin films were 2-(dimethylamino) ethyl methacrylate (DMAEMA, 97%, abcr, Germany), hydroxyethyl methacrylate (HEMA, 98%, abcr, Germany), *tert-butyl*-peroxide (TBPO, Sigma-Aldrich, Germany), 1,3,5-trivinyl-1,3,5-trimethylcyclo-trisiloxane (V3D3, 95%, abcr, Germany) and ethylene glycol dimethacrylate (EGDMA, 98%, abcr, Germany).

Polymer thin films of p(HEMA-co-EGDMA), p(HEMA-co-V3D3), p(DMAEMA-co-EGDMA), and p(DMAEMA-co-V3D3) were deposited on Si-wafers via iCVD with *tert-butyl*-peroxide (TBPO) as the initiator. The Si-wafers were cut into 3 mm x 3 mm pieces for preparation of samples for

antiviral and anticancer tests. For the evacuation of the reactor, a scroll pump (nXDS 10i, Edwards) was used. A nitrogen flow was introduced to the process by a mass flow controller (MC series, Alicat Scientific Inc.). For the precise control of the pressure, a capacitive manometer (Baratron, MKS) and a butterfly valve (615, VAT) were applied. A power supply (SM 7020-D, Delta Elektronika) was used to heat a NiCr filament array (Ni80/Cr20, Goodfellow). The samples were cooled by a circulating thermostat (CC-K6, Huber). pEGDMA thin films were deposited for 3 h by an EGDMA gas flow of 0.3 sccm, a TBPO gas flow of 0.3 sccm, and a nitrogen gas flow of 0.2 sccm while maintaining a process pressure of 40 Pa. 42 W was applied to the filament array to start the reaction. A substrate temperature of 30 °C was maintained throughout the entire deposition process. p(HEMA-co-EGDMA)/p(DMAEMA-co-EGDMA) thin films were deposited for 3 h by a HEMA/DMAEMA gas flow of 0.1 sccm, an EGDMA gas flow of 0.2 sccm, a TBPO gas flow of 0.3 sccm and a nitrogen gas flow of 0.2 sccm. The process pressure was 40 Pa and 42 W was applied to the filament array while the substrate temperature was kept at 30 °C. The pV3D3 thin films were deposited for 3 h using a V3D3 gas flow of 0.45 sccm, a TBPO gas flow of 0.3 sccm, and a nitrogen gas flow of 0.2 sccm. The process pressure, filament power, and substrate temperature were 40 Pa, 42 W 30 °C, respectively. For the p(HEMA-co-V3D3) thin film deposition a HEMA/DMAEMA gas flow of 0.15 sccm, a V3D3 gas flow of 0.3 sccm, a TBPO gas flow of 0.3 sccm, and a nitrogen gas flow of 0.2 sccm were used to deposit the thin films. The deposition time was 3 h and process pressure, filament power, and substrate were again kept at 40 Pa, 42 W, and 30 °C, respectively.

Thin Film Characterization Methods: A Fourier-transform infrared (FTIR) spectrometer (Vertex 80v, Bruker) was used to measure the characteristic bands and peaks of the prepared polymers from 500 cm⁻¹ to 4000 cm⁻¹ with a step width of 4 cm⁻¹. XPS measurements (Omicron Nano-Technology) were performed with an Al K-alpha X-ray source, an X-ray tube power of 252 W, and a pass energy of 30 eV. An AFM (alpha300 RA -Raman-AFM- Microscope, WITec) was used to measure the surface topography using AC240 TS AFM tips (Asylum Research) in AC Mode. Afterward, the software Gwyddion was used to calculate the root mean square roughness of the measured areas. A self-built water contact angle (WCA) measurement setup was used to measure the wetting via sessile drop technique with 5 µL droplets, controlled by a step-motor connected to a syringe containing deionized water. The thin film thickness was measured by an ellipsometer (M-2000UI, EC-400 J.A. Woollam Co. Inc) and a profilometer (DektakXT, Bruker).

Biological Investigations: Cell lines: The used cell lines included the VERO cell line (normal monkey kidney cells) and HepG2 cell line (ATCC, USA). Other chemicals and reagents were used including growth media (GM); Dulbecco's modified Eagle's medium (DMEM), DMEM-glucose with L-glutamine medium supplemented with 10% fetal bovine serum, antibiotics (2% penicillin-streptomycin, 200 IU mL⁻¹), 1% NEAA, 3% NAHCO₃ and 1% sodium pyruvate. Also, maintenance media (MM) was used where the same components were added except for 2% fetal bovine serum. Additional chemicals included Trypsin EDTA (0.025% trypsin and 0.0025% EDTA), phosphate buffer saline (PBS), and 3-(4,5-dimethylthiazol-2-yl)-2,5-diphenyltetrazolium bromide (MTT dye) which were purchased from Serva (Heidelberg, Germany). The cells were incubated at 37 °C with a 5% CO₂ incubator and sub-cultured by trypsinization.

Human fibroblasts were isolated from gingival tissues from the patients who underwent oral surgical interventions in the Department of Oral and Maxillofacial Surgery at Christian-Albrechts-University in Kiel, Germany. (The extraction protocol was conducted according to the guidelines of the Declaration of Helsinki and approved by the Institutional Ethics Committee of the Medical Faculty of Christian Albrechts University, Kiel-Germany /protocol code D640/20.) Briefly, adherent gingival tissues were mechanically removed from the specimens, cut into fragments of 0.3–0.5 cm in diameter, and extensive washing in phosphate-buffered solution (pH:7.4) was performed. The fragments were seeded as explants into the culture flasks and cultivated at 37 °C in a humidified atmosphere of 95% air and 5% CO₂. Dulbecco's modified eagle's medium, supplemented with fetal calf serum,

100 000 mg L⁻¹ penicillin, 100 mg L⁻¹ streptomycin, 2 mM L-glutamine, 100 nM dexamethasone and 1 mM L-ascorbic acid 2-phosphatase (Sigma, Deisenhofen, Germany) was used for cultivation. Cells were subcultures in a second passage at a density of $3.3 \times 1\,000\,000$ cm⁻². For the second passage, a cell dispenser was used to bring the cells into suspension. One hundred microliters containing $3.3 \times 100\,000$ fibroblast-like cells in the second passage were transferred onto the samples.

In silico study methods: The in silico study was performed prior to in vitro testing of the proposed ligands against SARS-CoV-2 target proteins (Spike, ACE2 proteins). Furthermore, against cancer BCL2 target protein (B-cell lymphoma 2) encoded in humans by the BCL2 gene (key regulators of the intrinsic apoptotic pathway), was the founding member of the Bcl-2 family of regulator proteins where its downregulation-induced anti-proliferative activity indicating anticancer activity. HDock server was utilized for protein-ligand interaction,^[52] the screening method was restricted to molecular docking to study the binding difference between the molecules.^[53] For molecular docking, the structures of the ligands (pV3D3 on Si, p(DMAEMA-co-V3D3) on Si, p(HEMA-co-V3D3) on Si, pEGDMA on Si, p(DMAEMA-co-EGDMA) on Si and p(HEMA-co-EGDMA) on Si) were built by using Swiss ADME, the MMFF94 force field and energy minimization by using Avogadro software. Structures of (Spike, ACE2, and Bcl2 proteins) were taken from the protein data bank (i.e., PDB ID (6vw1, 1R42 and 2W3L)) and proteins were prepared by AutoDock Vina. Remdesivir was a positive control to compare it with the targeted materials. Molecular docking was used to study the binding difference between the molecules.^[54]

Anti-proliferative activity against cancer cells: The cytotoxicity effect was evaluated for the studied materials and IC50 was determined on both human liver cancer cells (HepG2) and human breast cancer cells (MCF-7, not mentioned in results) using MTT colorimetric assay. All results were compared with paclitaxel as a positive control which was used as a traditional cancer therapy. In addition, all materials were evaluated on Vero cells (monkey kidney cells) as a normal control to prove anti-proliferative activity against cancer cells according to a previously published protocol.^[55] Before testing antiviral activity against human adenovirus 5 (ADV5) and SARS-CoV2, the cytotoxicity of the proposed materials was determined on both vero and vero E6 cell lines, respectively, using the same assay. To understand the anti-cancer invasive behavior a migration assay was performed on HepG2 treated with the iCVD polymers. HepG2 cells were seeded into 12-well tissue culture plates at a density of 200 000 cells per well and then incubated in a CO2 incubator until reaching 90% confluency. The scratch was performed in a straight line with a 100 μ L pipette tip and washed gently with PBS to remove any debris or clumps from the cells. Then 1 mL fresh medium was added for every well to detect their ability to migrate.^[50] Afterward, images were obtained by a digital camera (Axiocam 512 Color, Carl Zeiss, Germany) and compared with cell control images at 0, 24, and 48 h. The gaps for every scratch were determined by ZEN2.3 image-analysis software and gap closures were determined after 24 and 48 h.

Regarding the apoptotic effect, molecular investigations were performed using quantitative real-time PCR assays on HepG2 treated with the tested materials. Cells at a density of 5×10^4 cells mL⁻¹ were seeded into a 6-well plate. After 24 h, the cells were treated with the polymer materials and incubated for 24 h or 3 days.^[56] When the cytotoxic effect was presented by rounding of cells, cells were trypsinized and pellets were collected, washed, and stored at -80 °C for investigating some apoptotic gene expression using quantitative real-time PCR^[57] which was performed as follows: Gene Jet RNA purification kit (Thermo Scientific, Inc, USA) was used for total RNA extraction according to the manufacturer's instructions as used in a previous study.^[55] First-strand cDNA was synthesized using oligodT primers and the RevertAid Reverse Transcriptase kit (Thermo Scientific, USA). PCR was run by a quantitative real-time detection system (Applied Biosystems 7500 Fast Real-Time PCR system Thermal Cycling Block, USA). Amplification was performed under the following conditions: 1 min at 95 °C, 40 cycles at 95 °C for 1 min, 58 °C for 1 min, and 72 °C for 2 min. Post amplification melting temperature (T_m) analysis, clearly differentiated nonspecific PCR products. Negative controls (nontemplate water instead of cDNA) were also included to ensure the lack

of DNA reagent contamination. The Q-PCR data were analyzed using the comparative CT method.^[58] Briefly, the difference in cycle threshold, ΔCT , was determined as the difference between the tested gene and human GAPDH. Then, $\Delta\Delta CT$ was obtained by finding the difference between the two groups. The fold change (FC) was calculated as $2^{-\Delta\Delta CT}$.

Anti-viral activity: The followed protocol for an antiviral assay against human adenovirus type 5 was used according to the previously published report as follows:^[31]

Regarding virucidal mechanisms, Vero cells were seeded into a 6-well plate at a cell density of 5×10^5 cells/well, then incubated for 24 h at a 5% CO₂ incubator until obtaining ≈ 80 –90% confluent sheet. On the second day, the cells were treated with the tested materials after their incubation with 100TCID50 of viral load at 4 °C for 1 h, then treated cells were incubated for 24 h. The viral load was detected using a quantitative PCR assay.^[59,31] Such a mechanism indicated the ability of the tested material to neutralize the virus and prevent its replication into infected cells. Regarding viral adsorption mechanisms, Vero cells were seeded into a 6-well plate (5×10^5 cells mL⁻¹), then incubated for 24 h at a 5% CO₂ incubator. On the second day, the cells were treated with the proposed materials and then incubated for another 24 h. On the third day, the cells were infected with 100 TCID50 of the virus then after 24 h and then subjected to real-time PCR assay to detect viral load.^[60] The polymer iCVD thin films were also tested for antiviral activity against SARS-CoV2 using a CoviDrop SARS-CoV-2 Spike-ACE2 Binding Inhibitor Screening assay. Anti-SARS-CoV-2 was carried out using CoviDrop SARS-CoV-2 Spike-ACE2 Binding Inhibitor Screening commercial Fast Kit (EpiGentek, USA). The entry of SARS-CoV-2 into the human host cells occurred through the binding of surface unit S1 of its spike protein to the cell receptor angiotensin-converting enzyme 2 (ACE2). Therefore, the method was based on pre-coating of SARS-CoV-2 spike protein onto microplate wells. Its tagged ACE2 was bound to the coated spike protein in the presence or absence of inhibitors. The amount of the bound ACE2, which was proportional to ACE2 inhibition intensity, could be recognized afterward by the binding detection solution containing anti-His antibody and measured through an ELISA-like reaction by reading the absorbance in a microplate spectrophotometer at a wavelength of 450 nm. The binding activity of ACE2 was proportional to the measured optical density (OD) intensity. Generally, the more the ACE2 binding was inhibited, the lower the OD intensity was determined. Methods were carried out according to the manufacturer's instructions.

Analysis of cell viability, immunostaining, and fluorescence imaging of human fibroblasts: To assess the viability of human fibroblasts on samples, MTT assays were conducted after 24 h. Briefly, 96-well microtiter plates with 5×10^3 cells per well were incubated and a sample of 100 μ L eluate was obtained to identify the metabolically active cells via the in vitro Cell Proliferation KIT 1 (Roche, 11465007001, Mannheim, Germany). The optical density of the samples was measured photometrically^[54] at 450 nm wavelength. Bare glass served as the control. The viability of the fibroblasts was identified by staining with fluorescein diacetate (FDA, Sigma-Aldrich, St. Louis, MO, USA) and propidium iodide (PI, Sigma-Aldrich, St. Louis, MO, USA). Eight-well plates with 1×10^4 cells per well were supplied with a standard nutrient medium. The cells were washed with PBS and stained with the FDA solution containing 30 μ L of stock solution (1 mg FDA mL⁻¹ acetone) diluted in 10 mL PBS. After an incubation period of 15 min at 37 °C in the dark environment, the FDA solution was removed and replaced by 500 μ L PI stock solution. After an incubation time of 120 s, the cells were washed twice with PBS. Within 60 min after staining, the cells were examined via a fluorescence microscope (Axioplan2) and documented with a digital camera (AxioCam MRc5 from ZEISS, Oberkochen, Germany). The dyes could be excited at 488 nm (blue light, argon laser). The green fluorescence (FDA) was detected at 530 nm, whereas the red fluorescence (PI) was detected at 620 nm.

Supporting Information

Supporting Information is available from the Wiley Online Library or from the author.

Acknowledgements

The authors would like to thank the German Research Foundation for funding through the RTG 2154 (project number 270394294) via project P4, the SFB 1261 (project number 286471992) via project A2 and KiNSIS (Kiel Nano, Surface and Interface Science). The authors also acknowledge partial funding of this research through the German Federal Government via the ZIM project "Clean Window" KK5010203WZ1. A.A. would like to thank DAAD for her funded scholarship at Kiel University under the supervision of F.F.

Open access funding enabled and organized by Projekt DEAL.

Conflict of Interest

The authors declare no conflict of interest.

Data Availability Statement

The data that support the findings of this study are available from the corresponding author upon reasonable request.

Keywords

antiviral activity, bio-interface, in silico, in vitro anticancer, initiated chemical vapor depositions, polymer thin films, SARS-CoV-2

Received: July 12, 2023

Revised: September 13, 2023

Published online:

- [1] A. Sionkowska, *Prog. Polym. Sci.* **2011**, *36*, 1254.
- [2] J. Li, D. J. Mooney, *Nat. Rev. Mater.* **2016**, *1*, 16071.
- [3] H. Mehrdad, A. Azadi, P. Rafiel, *Adv. Drug Delivery Rev.* **2008**, *60*, 1638.
- [4] T. R. Hoare, D. S. Kohane, *Polymer* **2008**, *49*, 1993.
- [5] E. Ramírez, S. G. Burillo, C. Barrera-Díaz, G. Roa, B. Bilyeu, *J. Hazard. Mater.* **2011**, *192*, 432.
- [6] N. G. Kandile, A. S. Nasr, *Carbohydr. Polym.* **2009**, *78*, 753.
- [7] K. Y. Lee, D. J. Mooney, *Chem. Rev.* **2001**, *101*, 1869.
- [8] J. L. Drury, D. J. Mooney, *Biomaterials* **2003**, *24*, 4337.
- [9] Y. Chen, S. Zhang, Q. Cui, J. Ni, X. Wang, X. Cheng, H. Alem, P. Tebon, C. Xu, C. Guo, R. Nasiri, R. Moreddu, A. K. Yetisen, S. Ahadian, N. Ashammakhi, S. Emaminejad, V. Jucaud, M. R. Dokmeci, A. Khademhosseini, *Lab Chip* **2020**, *20*, 4205.
- [10] D. Buenger, F. Topuz, J. Groll, *Prog. Polym. Sci.* **2012**, *37*, 1678.
- [11] K. K. Gleason, *CVD polymers: fabrication of organic surfaces and devices*, John Wiley & Sons, Hoboken, NJ **2015**.
- [12] K. K. Gleason, *Front Bioeng Biotechnol* **2021**, *9*, 632753.
- [13] M. Alf, A. Asatekin, M. C. Barr, S. H. Baxamusa, H. Chelawat, G. Ozaydin Ince, C. D. Petruczok, R. Sreenivasan, W. E. Tenhaeff, N. J. Trujillo, S. Vaddiraju, J. Xu, K. K. Gleason, *Adv. Mater.* **2010**, *22*, 1993.
- [14] S. J. Yu, K. Pak, M. J. Kwak, M. Joo, B. J. Kim, M. S. Oh, J. Baek, H. Park, G. Choi, D. H. Kim, J. Choi, Y. Choi, J. Shin, H. Moon, E. Lee, S. G. Im, *Adv. Eng. Mater.* **2018**, *20*, 1700622.
- [15] K. Yilmaz, H. Sakalak, M. Gursoy, M. Karaman, *Ind. Eng. Chem. Res.* **2019**, *58*, 14795.
- [16] H. Sakalak, K. Yilmaz, M. Gürsoy, M. Karaman, *Chem. Eng. Sci.* **2020**, *215*, 115466.
- [17] C. Cheng, M. Gupta, *Ind. Eng. Chem. Res.* **2018**, *57*, 11675.
- [18] M. Gupta, K. K. Gleason, *Thin Solid Films* **2016**, *515*, 1579.
- [19] S. Schröder, A. M. Hinz, T. Strunskus, F. Faupel, *J Phys Chem A* **2021**, *125*, 1661.
- [20] S. H. Baxamusa, S. G. Im, K. K. Gleason, *Phys. Chem. Chem. Phys.* **2009**, *26*, 5227.
- [21] S. Schröder, O. Polonskyi, T. Strunskus, F. Faupel, *Mater. Tod.* **2020**, *37*, 35.
- [22] P. Chen, Z. Zhang, Z. Rouse, S. P. Baker, J. Yeo, R. Yang, *Nat Synth* **2023**, *2*, 373.
- [23] H. Moon, H. Seong, W. C. Shin, W. T. Park, M. Kim, S. Lee, J. H. Bong, Y. Y. Noh, B. J. Cho, S. Yoo, S. G. Im, *Nat. Mater.* **2015**, *14*, 628.
- [24] J. H. Koo, J. Kang, S. Lee, J. Song, J. Choi, J. Yoon, H. J. Park, S. Sunwoo, D. C. Kim, W. Nam, D. Kim, S. G. Im, D. Son, *Nat. Electron.* **2023**, *6*, 137.
- [25] K. Chan, K. K. Gleason, *Langmuir* **2005**, *21*, 8930.
- [26] R. K. Bose, K. K. S. Lau, *Chem. Vap. Depos.* **2009**, *15*, 150.
- [27] P. Materna, D. Illek, K. Unger, M. Thonhofer, T. M. Wrodnigg, A. M. Coclite, *Monatshefte für Chemie-Chemical Monthly* **2023**, *154*, 373.
- [28] M. Lee, D. Chun, S. Park, G. Choi, Y. Kim, S.-J. Kang, S. G. Im, *Small* **2022**, *18*, 2106648.
- [29] W. Reichstein, L. Sommer, S. Veziroglu, S. Sayin, S. Schröder, Y. K. Mishra, E. I. Saygili, F. Karayürek, Y. Açil, J. Wiltfang, A. Gülses, F. Faupel, O. C. Aktas, *Polymers* **2021**, *13*, 186.
- [30] R. Yang, K. K. Gleason, *Langmuir* **2012**, *28*, 12266.
- [31] S. A. Loutfy, A. I. Abdel-Salam, Y. Moatasim, M. R. Gomaa, N. F. Abdel Fattah, M. H. Emam, F. Ali, H. A. Elshehaby, E. A. Ragab, H. M. Alam El-Din, A. Mostafa, M. A. Ali, A. Kasry, *RSC Adv* **2022**, *12*, 15775.
- [32] K. K. S. Lau, Z. Chen, US20220372201A1 **2022**.
- [33] M. H. Burk, S. Schröder, W. Moormann, D. Langbehn, T. Strunskus, S. Rehders, R. Herges, F. Faupel, *Macromolecules* **2020**, *53*, 1164.
- [34] V. Graur, A. Mukherjee, K. O. Sebakhly, R. K. Bose, *Polymers* **2022**, *14*, 3393.
- [35] K. Jung, N. Corrigan, E. H. H. Wong, C. Boyer, *Adv Mater* **2021**, *34*, 2105063.
- [36] Z. Terzopoulou, A. Zamboulis, I. Koumentakou, G. Michailidou, M. J. Noordam, D. N. Bikiaris, *Biomacromolecules* **2022**, *23*, 1841.
- [37] A. Akbari, A. Bigham, V. Rahimkhoei, S. Sharifi, E. Jabbari, *Polymers* **2022**, *14*, 1634.
- [38] R. H. Bianculli, J. D. Mase, M. D. Schulz, *Macromolecules* **2020**, *53*, 9158.
- [39] N. Jarach, H. Dodiuk, S. Kenig, *Polymers* **2020**, *12*, 1727.
- [40] S. Sajadimajd, R. Bahramsoltani, A. Iranpanah, J. Kumar Patra, G. Das, S. Gouda, R. Rahimi, E. Rezaeihamiri, H. Cao, F. Giampieri, M. Battino, R. Tundis, M. G. Campos, M. H. Farzaei, J. Xiao, *Pharmacol Res* **2020**, *151*, 104584.
- [41] R. Mansurnezhad, L. Ghasemi-Mobarakeh, A. M. Coclite, M. H. Beigi, H. Gharibi, O. Werzer, M. Khodadadi-Khorzoughi, M. H. Nasr-Esfahani, *Mater. Sci. Eng., C* **2020**, *110*, 110623.
- [42] W. S. O'Shaughnessy, D. J. Edell, K. K. Gleason, *Thin Solid Films* **2009**, *517*, 3612.
- [43] W. S. O'Shaughnessy, M. Gao, K. K. Gleason, *Langmuir* **2006**, *22*, 7021.
- [44] G. Socrates, *Infrared and Raman characteristic group frequencies: tables and charts*, John Wiley & Sons, Chichester, England **2004**.
- [45] P. Louette, F. Bodino, J. J. Pireaux, *Surf. Sci. Spect.* **2005**, *12*, 38.
- [46] A. Tavakoli, A. Ataei-Pirkooh, G. Mm Sadeghi, F. Bokharai-Salim, P. Sahrapour, S. J. Kiani, M. Moghoofei, M. Farahmand, D. Javanmard, S. H. Monavari, *Nanomedicine* **2018**, *13*, 2675.
- [47] C. Weiss, M. Carriere, L. Fusco, M. A. Capua, J. A. Regla-Nava, M. Pasquali, J. A. Scott, F. Vitale, M. I. A. Unal, C. Mattevi, D. Bedognetti, A. Merkoçi, E. Tasciotti, A. Yilmazer, Y. Gogotsi, F. Stellacci, L. G. Delogu, *ACS Nano* **2020**, *14*, 6383.
- [48] C. Bastiancich, P. Danhier, V. Préat, F. Danhier, *J. Controlled Release* **2017**, *243*, 29.
- [49] Z. Sun, K. (K.) Ostrikov, *Sust. Materials Technol.* **2020**, *25*, e00203.
- [50] X. Mei, J. Li, Z. Wang, D. Zhu, K. Huang, S. Hu, K. D. Popowski, K. Cheng, *Nat. Mater.* **2023**, *22*, 903.
- [51] R. Cheng, H. A. Santos, *Matter* **2022**, *5*, 1065.

- [52] Y. Yan, H. Tao, J. He, S. Y. Huang, *Nat. Protoc.* **2020**, *15*, 1829.
- [53] S. Y. Huang, X. Zou, *Nucleic Acids Res.* **2014**, *42*, e55.
- [54] Y. Yan, Z. Wen, X. Wang, S. Y. Huang, *Proteins: Struct., Funct., Bioinf.* **2017**, *85*, 497.
- [55] S. A. Loutfy, R. H. Shalaby, A. R. Hamed, M. B. Mohamed, A. Bakarat, Z. F. Abdullah, H. Yousef, A. Tamim, H. E. Eldin, M. Hegazy, *Chem Pharm Res* **2015**, *7*, 470.
- [56] A. R. Paek, C. H. Lee, H. J. You, *Mol. Carcinog.* **2014**, *53*, E161.
- [57] Y. Xue, T. Zhang, B. Zhang, F. Gong, Y. Huang, M. Tang, *J. Appl. Toxicol.* **2016**, *36*, 352.
- [58] T. D. Schmittgen, K. J. Livak, *Nat. Protoc.* **2008**, *3*, 1101.
- [59] H. Nageh, M. H. Emam, F. Ali, N. F. Abdel Fattah, M. Taha, R. Amin, E. A. Kamoun, S. A. Loutfy, A. Kasry, *ACS Omega* **2022**, *7*, 14887.
- [60] L. A. Osminkina, S. N. Agafilushkina, E. A. Kropotkina, N. Y. Saushkin, I. V. Bozhev, S. S. Abramchuk, J. V. Samsonova, A. S. Gambaryan, *Bioact Mater* **2022**, *7*, 39.